RESEARCH ARTICLE

NANO · MICRO small
www.small-journal.com

Rapid Yet Efficient Reduction of Graphene Oxide Triggered by Semi-Molten Metals

Jianpeng Liu, Wenchang Zhang, Chang Cheng, Juncheng Zhu, Tianle Wang, Kun Ni, Zifeng Lin, Zefeng Guan, Yanwu Zhu,* and Jiliang Zhu**

Reduced graphene oxide (rGO) has garnered extensive attention as electrodes, sensors, and membranes, necessitating the efficient reduction of graphene oxide (GO) for optimal performance. In this work, a swift reduction of GO that involves bringing GO foam in contact with semi-molten metals like tin (Sn) and lithium (Li) is presented. These findings reveal that the electrical resistance of GO foam is significantly diminished by its interaction with these metals, even in dry air. Taking inspiration from this technique, Sn foil is employed to encase the GO foam, followed by a calcination in 15 vol% H_2/Ar environment at 235 °C to fabricate the rGO, which demonstrates a remarkably lower electrical resistivity of 0.42 Ω cm when compared to the chemically reduced GO via hydrazine hydrate (650 Ω cm). The reduction mechanism entails the migration of Sn on GO and its subsequent reaction with oxygen functional groups. SnO/$Sn(OH)_2$ formed from the reaction can be subsequently reversed through reduction by H_2 to Sn. Utilizing this rGO as the host material for a sulfur cathode, a lithium–sulfur battery is constructed that displays a specific capacity of 1146 mAh g^{-1} and maintains a capacity retention of 68.4% after 300 cycles at a rate of 0.2 C.

1. Introduction

Reduced graphene oxide (rGO) is a crucial material for applications in various fields. Its properties such as excellent flexibility, high specific surface area and good electrical conductivity, make it an ideal candidate for use in flexible sensors, next-generation electrode materials, marine oil pollution adsorption, and 3D printing.[1] The reduction of graphene oxide (GO) is an essential step in the production of rGO. Several methods have been reported for the reduction of GO, including chemical reduction,[2] pyrolysis,[3] electrochemical reduction,[4] microwave reduction,[5] and flash reduction.[6] Commonly used chemical reductants often operate in strong acidic or alkaline environments. In suspension reduction, a substantial quantity of water is required during the reduction process and for subsequent cleaning of rGO, restricting the practical application of chemical reduction. Pyrolysis reduction of GO solid typically needs a high-temperature annealing, which releases CO/CO_2 gas[3] and generates defects that can negatively impact the electrical conductivity of rGO.[7]

Electrochemical reduction depends on GO films that undergo linear sweeping in a sodium phosphate buffer.[8] However, the morphology of rGO obtained through this method is restricted to thin films.[9] In the microwave reduction, GO absorbs microwaves and heats up rapidly, resulting in the removal of oxygen functional groups.[10] Hu et al. demonstrated that the rise of oxygen content in GO disrupts the π–π conjugate structure, which consequently makes the material less capable of absorbing microwaves.[11] Chhowalla et al. mentioned in the study on the reduction of GO using microwaves that a gentle reduction of GO is necessary before microwave irradiation, and the heat treatment conditions involved holding at 300 °C for 1 h.[5] Flash reduction typically involves the use of a photographic camera flash to achieve photothermal heating, which ultimately removes oxygen functional groups.[6] While flash reduction is quick, multiple flashes are required, and only the area that has been exposed to the flash is reduced.

Metals such as Al, Fe, and Zn have been employed to reduce GO, typically in the mixture of metal and acid.[12–14] Two possible mechanisms have been suggested for the reduction of GO using

J. Liu, C. Cheng, T. Wang, Z. Lin, Z. Guan, J. Zhu
College of Materials Science and Engineering
Sichuan University
Chengdu 610064, China
E-mail: jlzhu167@scu.edu.cn
W. Zhang, K. Ni, Y. Zhu
School of Chemistry and Materials Science
University of Science and Technology of China
Hefei, Anhui 230026, China
E-mail: zhuyanwu@ustc.edu.cn
J. Zhu
Hefei National Laboratory for Physical Sciences at Microscale
University of Science and Technology of China
Hefei, Anhui 230026, China
E-mail: jc1998@mail.ustc.edu.cn
Y. Zhu
Key Laboratory of Precision and Intelligent Chemistry
University of Science and Technology of China
Hefei, Anhui 230026, China

The ORCID identification number(s) for the author(s) of this article can be found under https://doi.org/10.1002/smll.202304502

DOI: 10.1002/smll.202304502

metals: 1) rapid electron transport between the metal and GO;[15] 2) hydrogen produced from the reaction between the metal and acid, which acts as a reducing agent. The reported reduction time using metals ranges from 30 minutes to several hours, depending on the specific reactants used. On the other hand, in solid-state reactions Lin et al. observed that GO turned from yellow to black after contacting molten Li metal and undergoing a rapid combustion.[16] It was inferred that H_2 generated from water reduced oxygen functional groups when GO came into contact with the molten Li. However, no further detailed studies have been conducted to examine the reduction mechanisms or the potential applications of rGO obtained by contacting GO with semi-molten metals.

Herein, we report a rapid yet efficient reduction of GO foam or film via contacting with semi-molten metals. We demonstrate that GO can be instantaneously reduced by contacting with Li/Sn at 220 °C in dry air. Our results show that the electrical resistivity of GO, as measured by a four-probe method, is significantly reduced from 1740.0 Ω cm to 1.81/1.92 Ω cm via point contact with semi-molten Li/Sn. Fourier transform infrared spectroscopy (FTIR) and X-ray photoelectron spectroscopy (XPS) measurements confirm the effective removal of oxygen functional groups. Furthermore, by wrapping GO with Sn foil and calcinating in 15 vol% H_2/Ar atmosphere at 235 °C, we obtained a sample named Sn-W-15%H-rGO, showing an electrical resistivity of 0.42 Ω cm, much lower than that of GO reduced by hydrazine hydrate (650 Ω cm). The FTIR and XPS results indicate the cooperative reduction effects of H_2 and Sn: H_2 reduces C—O groups, while Sn package reduces -OH groups and converts C═O to C—O. The density-functional-theory (DFT) calculations suggest that Sn atoms have the ability to migrate on GO, and the reaction between Sn and the oxygen functional groups is an exothermic process. Combining all the results, we infer the reduction process as the reaction of Sn atom with oxygen functional groups to form SnO or $Sn(OH)_2$, which is subsequently reduced by H_2. To further demonstrate the practical application of our approach, a Li–S battery is fabricated using Sn-W-15%H-rGO as the host material of S (Sn-W-15%H-rGO@S/Li, sulfur loading = 2 mg cm^{-2}), which exhibits a high gravimetric capacity of 1146 mAh g^{-1} and excellent stability for 300 cycles.

2. Results and Discussion

GO form or film in this work was synthesized via a modified Hummers' method (Supporting Information).[17,18] We reduced the GO in a glovebox via contact with semi-molten Li/Sn under Ar atmosphere at 220 °C, and the obtained rGO samples were named as Li-C-rGO-Ar and Sn-C-rGO-Ar (C denotes contact), respectively. In observation of the melting point of Li metal as 180 °C, we used a heating rate of 10 °C min^{-1} on the hotplate and a cooling rate exceeding 20 °C min^{-1} (Supporting Information). As shown in **Scheme 1**, Figure S2 and Videos S1 and S2, Supporting Information, when brown GO contacts with the semi-molten Li/Sn, the contact point rapidly turns black and extends on the entire sample in 0.2 s. The electrical resistivities measured by a four-probe method were 1.57 or 1.72 Ω cm for Li-C-rGO-Ar or Sn-C-rGO-Ar (Table S1, Supporting Information), respectively, much lower than that of GO (1740 Ω cm). For comparison, we also reduced GO using the chemical reduction method with hydrazine hydrate.[19] Intriguingly, the electrical resistivity of the chemically-reduced rGO (Chem-rGO, 650 Ω cm, Table S1, Supporting Information) is much higher than those of Li/Sn-C-rGO-Ar, suggesting superior reduction effect of the contact reduction in this work. We also conducted the reduction process using a commercial GO (Supporting Information) via point contact with Sn at 220 °C under Ar atmosphere. As shown in Video S3, Supporting Information, the color of commercial GO quickly turns from yellow to black as well.

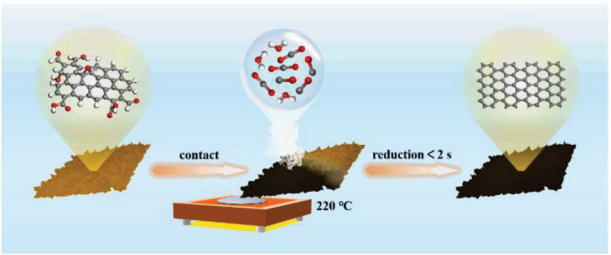

Scheme 1. Illustration of the point contact reduction of GO. The GO foam instantaneously turns black after point contact with semi-molten metals and white smoke is released during the process.

The TEM and SEM studies demonstrated that the morphology and lateral dimensions of Li/Sn-C-rGO-Ar (**Figure 1**a and Figure S3, Supporting Information) remain almost identical to those of GO (Figures 1b,c). The X-ray diffraction (XRD) pattern (Figure 1d) of the freeze-dried GO film shows a peak at 2θ = 9.65°, which is a typical diffraction peak of graphite oxide,[20] corresponding to an interlayer spacing of 0.917 nm. As a result of the removal of functional groups on GO, the interlayer spacings of Li/Sn-C-rGO-Ar were significantly reduced to 0.38 nm (2θ = 24°). The XRD pattern of Chem-rGO is similar to that of Li/Sn-C-rGO-Ar. The Raman spectra (Figure 1e) of GO film show D band at 1353.57 cm^{-1} and G band at 1596.94 cm^{-1},[21–23] while that of Li/Sn-C-rGO-Ar displays distinct D, G, 2D, and D + G bands.[21] The I_D/I_G values of Li/Sn-C-rGO-Ar are higher than that of GO, indicating that the removal of oxygen functional groups has induced defects in the resultant rGO.[11] In comparison, Chem-rGO exhibits a higher I_D/I_G value (1.158). The FTIR spectra (Figure 1f) reveals the presence of several oxygen functional groups in GO, including alkoxy C—O (1037 cm^{-1}), epoxy C—O (1171 cm^{-1}), C═O (1711 cm^{-1}), —OH (3287 cm^{-1}), —COOH, and aromatic C═C (1617 cm^{-1}).[10–25] In contrast, there was no peak observed at around 3300 cm^{-1} for Li/Sn-C-rGO-Ar, indicating a complete removal of -OH group. Additionally, the peak intensities of C═O group were significantly reduced compared to GO. The oxygen functional groups such as —OH and —COOH are extensively removed in Chem-rGO. Previous study shows that the chemical reduction can cause substantial structural damages and defects.[26] From XPS studies, Li-C-rGO-Ar and Sn-C-rGO-Ar have similar C/O ratios (4.3:1 and 4.5:1, respectively), while the C/O ratio of GO is 2.08:1 (Figure S1, Supporting Information). The C 1s XPS spectrum of Li/Sn-C-rGO-Ar confirms the absence of a peak corresponding to the C—OH bond, and much weaker peak intensities of the C—O bond (Figures S4 and S5, Supporting Information), consistent with the FTIR spectra. Interestingly, although the C/O ratio of Li/Sn-C-rGO-Ar measured by XPS was lower than that of Chem-rGO (6.4:1,

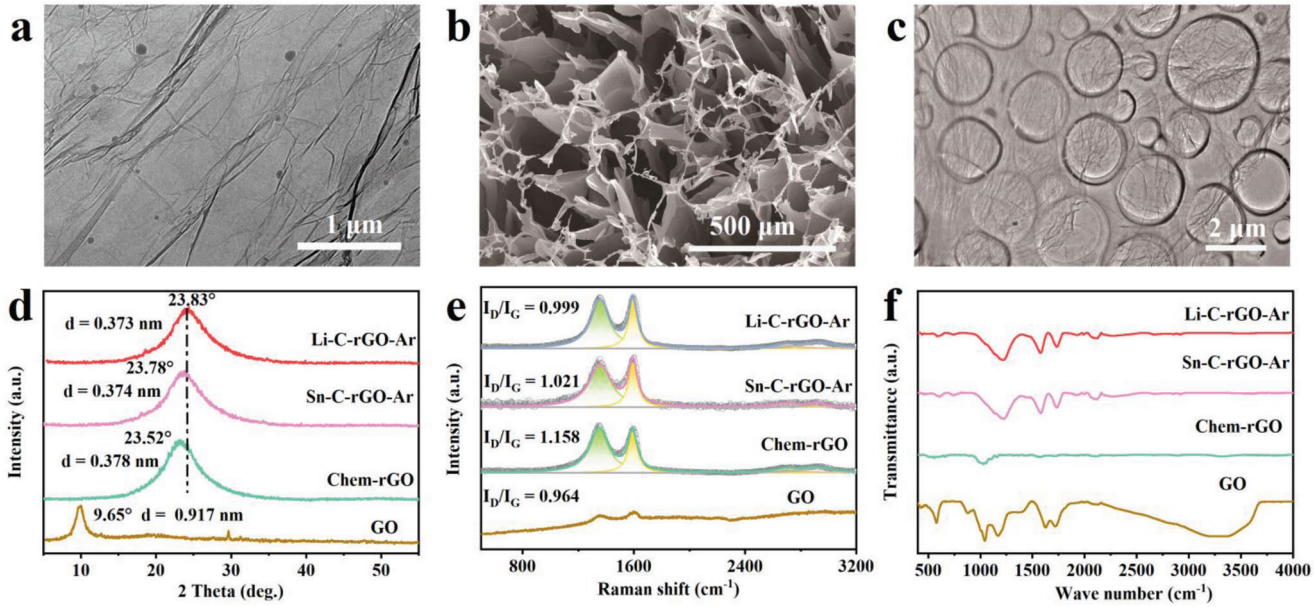

Figure 1. Characterizations of GO, Chem-rGO, and rGO via point contact reductions. a) Typical TEM image of Li-C-rGO-Ar. b) SEM and c) TEM images of GO. d) XRD patterns, e) Raman spectra, and f) FTIR spectra of Li-C-rGO-Ar, Sn-C-rGO-Ar, Chem-rGO, and GO.

Figure S6, Table S5, Supporting Information), the electrical resistivity of Chem-rGO was higher than that of Li/Sn-C-rGO-Ar. Compared to the reduction under an argon atmosphere, reduction in an oxygen containing atmosphere is more cost-effective. We reduced GO via point contact with Li/Sn under dry air at 220 °C. The obtained rGO exhibits a square resistance of 36.1 Ω sq^{-1} and an electrical resistivity of 1.81 Ω cm. (Table S1, Supporting Information), indicating that O_2 had minimal influence on the reduction effect. To understand the role of temperature we conducted contact reduction of GO with Li/Sn at 300 and 400 °C. The square resistance and electrical resistivity of the rGO are only slightly lower with increasing temperature (Table S1, Supporting Information), suggesting that temperatures over 220 °C had little impact on the reduction. Furthermore, we studied the impact of water vapor on the reaction by performing GO point contact with Sn at 220 °C in an ambient air atmosphere with a humidity > 50%. As shown in Figure S7 and Video S4, Supporting Information, only a small area of the GO film near the tip that comes into contact with Sn shows an obvious color change, while the rest of the flake remains brown. The square resistance and the electrical resistivity of the reduced sample are 27 600 Ω sq^{-1} and 1380 Ω cm, respectively. These results suggest that the presence of water vapor is highly negative on the point-contact reduction of GO. We deduce the reason as the higher heat conduction of water vapor during the GO reduction,[27,28] which could terminate the chain reaction.To further enhance the efficiency of reduction, GO foam was wrapped in Sn foil and calcinated at 235 °C under a 15 vol% H_2/Ar atmosphere.[29] After the system was cooled down naturally, we obtained the reduced GO denoted as Sn-W-15%H-rGO (W denotes wrap). The square resistance and the electrical resistivity of Sn-W-15%H-rGO are 8.4 Ω sq^{-1} and 0.42 Ω cm^{-1}, respectively, much lower than the corresponding values of Li/Sn-C-rGO-Ar. The SEM and TEM images of Sn-W-15%H-rGO show the thin films maintain the morphology (Figure S8, Supporting Information). To elucidate the roles of Sn and hydrogen in the reduction process, we calcinated GO at 235 °C under mixed atmospheres with varying concentrations of hydrogen (0, 5 vol%, 10 vol%, 15 vol%) with or without Sn packaging. The resulted samples are denoted according to the reaction conditions, as listed in the Supporting Information. As shown in Table S2, Supporting Information, when GO is calcinated in H_2/Ar atmosphere without Sn packaging, a higher H_2 concentrations leads to the improved electrical conductivity. But the square resistance and electrical resistivity of 15%H-rGO are still relatively high as 72.3 Ω sq^{-1} and 3.47 Ω cm^{-1}, respectively, about nine times higher than those of Sn-W-15%H-rGO. The XRD patterns of 5%H-rGO, 10%H-rGO, and 15%H-rGO show that the diffraction peak shifts to higher degrees as the H_2 ratio increased (**Figure 2**a), indicating the smaller interlayer spacing and more efficient removal of functional groups.[30] When the GO is reduced with Sn packaging under an H_2/Ar atmosphere, the XRD peak shifts to the higher degrees (Figure 2d), indicating a synergistic reduction effect of H_2 and Sn. As shown by the Raman spectra in Figure 2b,e and Table S3, Supporting Information, the I_D/I_G value decreases with the higher H_2 concentration. Furthermore, the I_D/I_G ratio is further reduced when GO is wrapped in Sn foil.

As observed in the FTIR spectra (Figure 2c,f), the —OH functional group is more effectively reduced with higher H_2 concentrations. However, a weak peak of —OH was still present for 15%H-rGO at 3450 cm^{-1}, indicating that hydrogen alone is not sufficient to completely remove —OH group. In contrast, a lower —OH signal is observed for Sn-W-rGO and no -OH peak found for Sn-5%H-rGO, suggesting that hydroxyl groups could be eliminated with the assistance of Sn packaging, even at a low H_2 ratio of 5%. The C═O group is also gradually reduced as H_2 ratio increases (Figure 2c,f and Table S4, Supporting Information). In comparison, the C═O peak intensity of the Sn-W-rGO is similar to that of GO, but the C═O peak intensity is greatly reduced

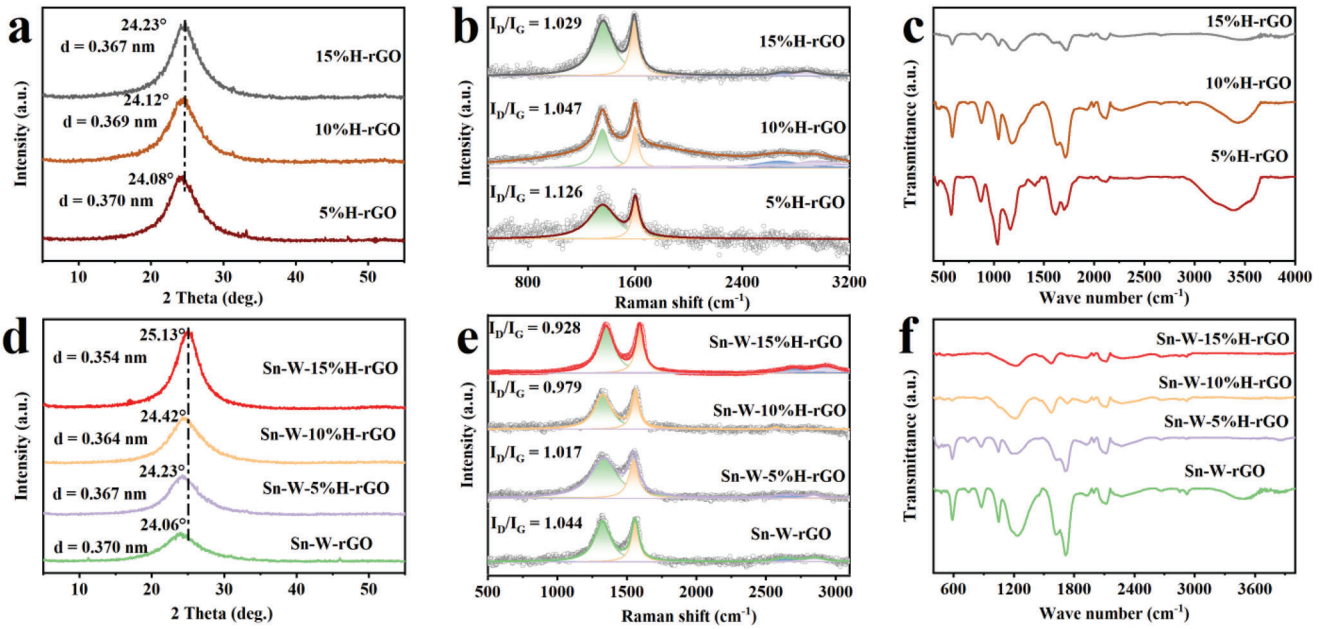

Figure 2. Characterizations of rGO samples after calcination under different reduction conditions. a) XRD patterns, b) Raman spectra, and c) FTIR spectra of 5%H-rGO, 10%H-rGO, and 15%H-rGO. d) XRD patterns, e) Raman spectra, and f) FTIR spectra of Sn-W-rGO, Sn-W-5%H-rGO, Sn-W-10%H-rGO, and Sn-W-15%H-rGO.

for the Sn-W-5%H-rGO (Figure 2f). These results indicate that the cooperative reduction effects of hydrogen and Sn can lead to the removal of different oxygen functional groups. The XPS measurements reveal that the C/O ratio of rGO increases with higher H_2 ratio when only H_2 is used for the reduction (Figures S9, S12 and Table S5, Supporting Information), while the peak intensities of C═O, C—O, and C—OH all decrease (Figures S10–S14, Supporting Information). Additionally, with higher H_2 concentration, the fraction of C—O is significantly decreased, C—OH unchanged, and C═O increased (Tables S6, S7, Supporting Information). As shown in Figures S5, S14 and Table S6, Supporting Information, Sn-W-rGO still displays a weak -OH signal, indicating an incomplete removal of -OH. Besides, the C═O fraction of Sn-W-rGO is much lower than that of Sn-C-rGO-Ar, implying a stronger reduction capability of C═O by Sn package (Table S4, Supporting Information). However, when Sn package is integrated with H_2/Ar atmosphere, the —OH signal is eliminated (Figure 2f), and the C/O ratio is also higher than that obtained via H_2/Ar reduction (Table S5, Supporting Information). Interestingly, with increasing H_2 ratio, the Sn-wrapped samples exhibited an increased C—O ratio and a decreased C═O ratio. This suggests that the Sn package could aid in converting C═O bonds to C—O bonds and prevent direct removal of C═O, which could result in defects in rGO.[31] This hypothesis is supported by the higher ratio of sp^2-C observed in the Sn-wrapped samples, indicating the effective restoration of π network in the rGO structure by Sn package.[1] The Sn 3d XPS demonstrates that, compared to the Sn before the reaction without H_2, the peak positions for Sn $3d_{3/2}$ and Sn $3d_{5/2}$ after the reduction both shift distinctly to the higher binding energies, indicating the oxidation of Sn (Figure S15, Supporting Information). Besides, the C/O ratio of Sn-W-rGO (2.8) is significantly lower than that of Sn-C-rGO-Ar (4.5). This suggests that as GO is reduced with the Sn package, the released species could oxidize the surface of Sn, thus lowering the effectiveness of the reduction. However, when an H_2/Ar mixed atmosphere is applied, the peaks of Sn $3d_{3/2}$ and Sn $3d_{5/2}$ only show a slight shift, indicating that H_2 serves a protective role for Sn against the oxidation (Figure S15, Supporting Information). To evaluate the feasibility of the approach, we carried out the cycling reduction using the same Sn foil for the reduction of fresh GO samples. As illustrated in Table S8, Supporting Information, after ten reduction processes, the reduced GO still exhibits a low electrical resistivity of 1.62 Ω cm, suggesting that Sn foil could be recycled and reused. Furthermore, we wrapped a commercial GO in Sn foil and calcinated the samples under a 15 vol% H_2/Ar atmosphere. As depicted in Figure S16, Supporting Information, the sample displays a distinctive color change after the reduction.

In order to explore the mechanism for the rapid reduction of GO with Sn, density functional theory calculations were conducted. A 4 × 4 supercell of single layer graphene was used, with an additional epoxy group or a hydroxyl group, to study the reaction of oxygen-containing groups on GO and Sn atom, as depicted in **Figure 3**. The reaction between Sn atom and epoxy group occurs immediately when the Sn atom is close enough, as shown in Figure 3a,b and Video S5, Supporting Information. There is no energy barrier presented in this reaction (shown in Figure S17, Supporting Information). The reaction is an exothermal process with −1.07 eV in enthalpy change. Regarding the reaction between Sn atoms and hydroxyl groups, the situation is quite similar, with no reaction energy barrier and an exothermic process with −1.18 eV in enthalpy change, as shown in Figure 3c,d, Figure S17 and Video S6, Supporting Information. The released energy could potentially heat and promote the further reductions of GO. The adsorption energy of the products on graphene exhibits a strength between physical and chemical adsorption, with value of −0.38 eV for SnO and −1.24 eV for

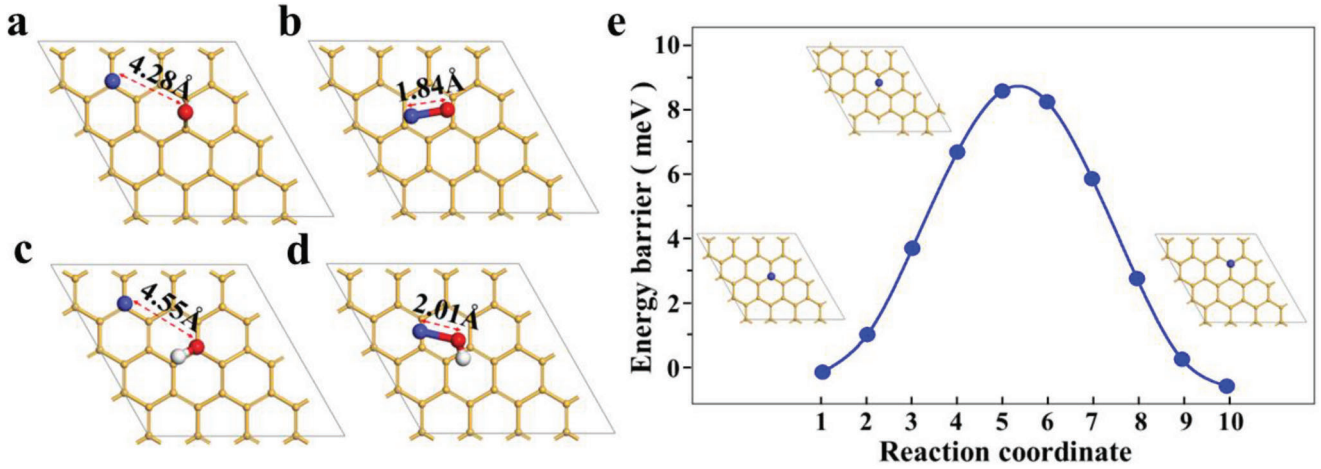

Figure 3. Sn atom on GO sheet with an epoxy group a) before and b) after geometry optimization; Sn atom on GO sheet with a hydroxyl group c) before and d) after geometry optimization; e) energy barrier for Sn migration on the graphene. Blue balls denote Sn atom, red balls denote O atom, yellow balls denote C atom, and white balls denote H atom.

SnOH. In addition, Sn atom shows low migration energy barrier (8.36 meV) on graphene along top-bridge-top sites, as presented in Figure 3e, indicating that the Sn atom can rapidly diffuse on graphene. Considering the experimental condition of H_2 atmosphere, the Gibbs energy change of reaction between SnO and H_2 is calculated to be −3.15 eV under 508 K, indicating that the reduction of SnO to Sn can occur spontaneously. Furthermore, the cohesive energy for Sn (−3.32 eV) is much greater than the adsorption energy of Sn on graphene (−0.38 eV), resulting in the aggregation of the reduced Sn atoms back to bulk phase. Combining experimental measurements with theoretical simulations, it is inferred that Sn acts as a catalyst and the GO reduction follows the following process: Sn atoms diffuse on the carbon matrix of GO, react with oxygen functional groups, and generate heat, which further promotes the reaction. The resulting SnO and $Sn(OH)_2$ can be readily reduced by hydrogen gas. Afterward, the Sn atoms regather back into the bulk phase. Typically, when specific oxygen functional groups such as ether bonds and epoxy groups are removed, CO/CO_2 is generated, and defects like carbon vacancies are created. This reduction process avoids the direct removal of oxygen functional groups into the gas phase, thus significantly reducing the number of defects.

To demonstrate the potential applications of the reduction method, we utilized Sn-W-15%H-rGO as the cathode host material for lithium-sulfur (Li–S) batteries (Supporting Information). The assembled battery is labeled as Sn-W-15%H-rGO@S/Li. For comparison, we also used chemically reduced GO as the host material of S to assemble Li–S batteries (Chem-rGO@S/Li). Cycling voltammetry (CV) tests were conducted on the batteries at a rate of 0.1 mV s^{-1}. As shown in **Figure 4**a, during the cathodic scans, two peaks are observed corresponding to the conversion of S_8 to Li_2S_x ($4 < x < 8$, high potential) and further reduction of Li_2S_x ($4 < x < 8$) to Li_2S_2 and Li_2S (low potential),[32] respectively. Additionally, two adjacent peaks during the anodic scans are ascribed to the oxidation of Li_2S_2 and Li_2S to Li_2S_x ($4 < x < 8$, low potential), and then to S_8 (high potential), respectively.[33] The difference in potential between the oxidation peak and the reduction peak of Sn-W-15%H-rGO@S/Li is smaller than that of Chem-rGO@S/Li, suggesting that Sn-W-15%H-rGO@S/Li shows the better reversibility and weaker polarization. We further conducted CV tests of the two batteries at different scan rates (Figure 4b,c). As the scan rate increases, polarization of Chem-rGO@S/Li is significantly higher than that of Sn-W-15%H-rGO@S/Li. For the same scan rate, the response current of Chem-rGO@S/Li is lower than that of Sn-W-15%H-rGO@S/Li. The CV results suggest that Sn-W-15%H-rGO@S/Li possesses stronger electrochemical kinetics.[34]

The charge–discharge tests (Figure S18a, Supporting Information) reveal that Sn-W-15%H-rGO@S/Li has three discharge stages, which is consistent with the results obtained from the CV tests. On the other hand, the Chem-rGO@S/Li battery shows a significant voltage drop during the second discharge stage and does not show a clear third discharge stage. Furthermore, the Sn-W-15%H-rGO@S/Li exhibits a higher gravimetric capacity of 1146 mAh g^{-1}, which is greater than that of the Chem-rGO@S/Li battery (1001 mAh g^{-1}). Additionally, the Sn-W-15%H-rGO@S/Li battery displays a smaller voltage difference between the charge and discharge plateaus, suggesting reduced cell polarization.[35] We also conducted electrochemical impedance spectroscopy (EIS) for both batteries. R_e is the sum of electrical resistance of electrolyte and electrode material, while R_{ct} is the charge transfer resistance of the cathode.[36] As shown in Figure 4d, Figure S19 and Table S9, Supporting Information, R_{ct} of Sn-W-15%H-rGO@S/Li is 61.2 Ω, lower than that of Chem-rGO@S/Li (90.85 Ω), suggesting the better electron transfer dynamics. The cycling performances of the two batteries were measured. As demonstrated in Figure 4e, the Sn-W-15%H-rGO@S/Li retains a high gravimetric capacity of 739 mAh g^{-1} after 300 cycles with a columbic efficiency of near 100%. However, the capacity of Chem-rGO@S/Li dramatically decreases after 170 cycles, and the columbic efficiency also fluctuates. When the charge/discharge rate is increased to 0.3 and 0.5 C, the voltage difference of Chem-rGO@S/Li increases to 0.26 and 0.42 V, respectively. In contrast, the voltage difference of Sn-W-15%H-rGO@S/Li remains relatively constant at 0.16 to 0.20 V (Figure S18b,c, Supporting Information). Furthermore, as the discharge

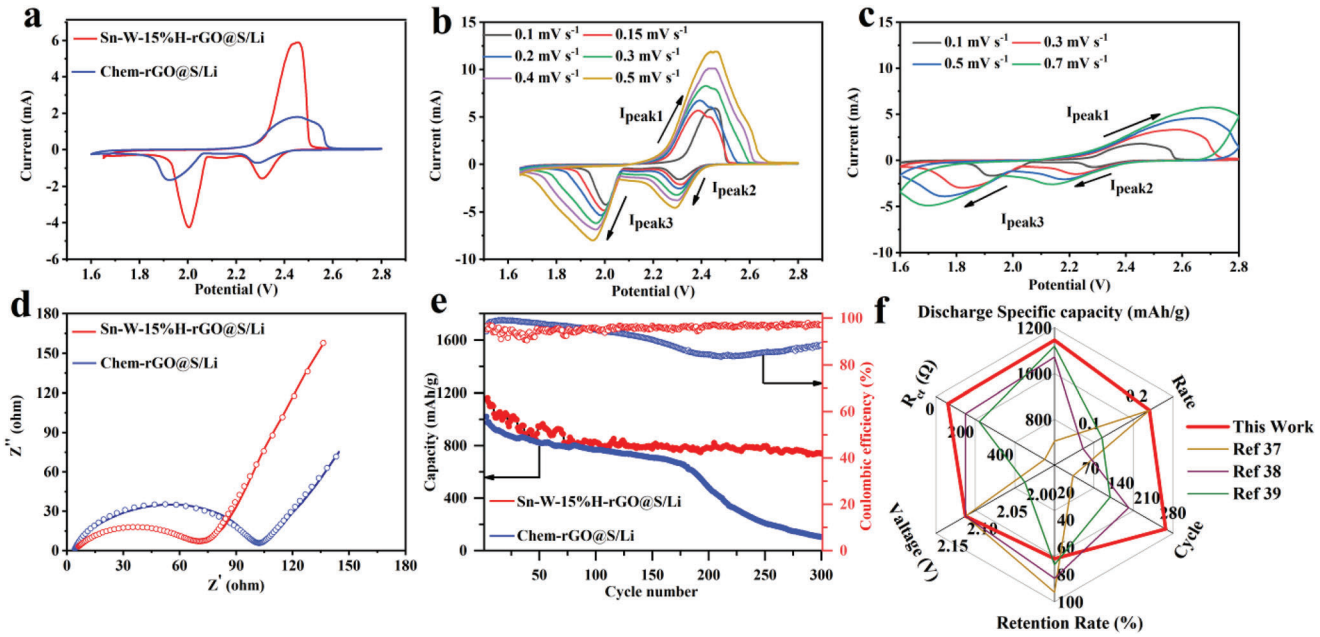

Figure 4. Electrochemical performance of Sn-W-15%H-rGO@S/Li and Chem-rGO@S/Li batteries. a) CV tests of Sn-W-15%H-rGO@S/Li and Chem-rGO@S/Li batteries at a scan rate of 0.1 mV s^{-1}. Rate-dependent CV measurements of b) Sn-W-15%H-rGO@S/Li and c) Chem-rGO@S/Li. d) Nyquist plots of Sn-W-15%H-rGO@S/Li and Chem-rGO@S/Li. e) Cycling performances of Sn-W-15%H-rGO@S/Li and Chem-rGO@S/Li at a rate of 0.2 C. f) Comparison chart of the electrochemical performance between Sn-W-15%H-rGO@S and other works.

rate increases, the decay magnitude and rate of the discharge specific capacity for Chem-rGO@S/Li are higher compared to Sn-W-15%H-rGO@S/Li (Figure S18d,e, Supporting Information). These results indicate the better cycling stability of the fabricated Sn-W-15%H-rGO@S/Li. Compared to the traditional chemical reduction approach, the rGO-based cathode synthesized by the reduction in this work demonstrate the lower cell polarization, lower electron transfer resistance, higher Li^+ diffusion constant as well as better electrochemical stability. Figure 4f shows a comparison of the electrochemical performance between Sn-W-15%H-rGO@S and other works that only use rGO as the host material.[37–39] The Sn-W-15%H-rGO@S exhibits significant improvement in charge transfer resistance, discharge rate, and cycle life, implying the potential application of this reduction method and rGO obtained.

3. Conclusion

In conclusion, we demonstrate that graphene oxide can be rapidly reduced via contact with semi-molten metals. The GO foam was reduced within 0.2 s by point contact with semi-molten Sn and Li. The resultant Li/Sn-C-rGO-Ar exhibited much lower electrical resistivities than Chem-rGO due to the lower number of defects generated during the reduction process. GO was then wrapped in Sn foil and calcinated the sample in a 15 vol% H_2/Ar atmosphere for more efficient removal of oxygen functional groups. The Sn package and H_2/Ar atmosphere exhibited synergistic reduction effects towards different oxygen functional groups, and the H_2/Ar atmosphere prevented the oxidation of Sn foil by the released oxidative species. DFT calculations indicated that Sn can easily migrate on GO and react with oxygen functional groups. As a result, the Sn-W-15%H-rGO demonstrated much better electrical conductivity. Additionally, the Li–S battery synthesized using Sn-W-15%H-rGO as the cathode host material showed a high gravimetric capacity of 1146 mAh g^{-1} and satisfactory cycling stability. Thus, this work presents a new way for the mass production of reduced graphene oxide with desirable physiochemical properties.

Supporting Information

Supporting Information is available from the Wiley Online Library or from the author.

Acknowledgements

This research was supported by the National Natural Science Foundation of China (Grant #52072250) and the Fundamental Research Funds for Central Universities (Grant #20826041E4245).

Conflict of Interest

The authors declare no conflict of interest.

Data Availability Statement

Research data are not shared.

Keywords

electrical resistivity, graphene oxide, reduction, tin

Received: May 30, 2023
Revised: July 30, 2023
Published online: August 30, 2023

[1] D. Chen, H. Feng, J. Li, *Chem. Rev.* **2012**, *112*, 6027.
[2] D. R. Dreyer, S. Park, C. W. Bielawski, R. S. Ruoff, *Chem. Soc. Rev.* **2010**, *39*, 228.
[3] C. Mattevi, G. Eda, S. Agnoli, S. Miller, K. A. Mkhoyan, O. Celik, D. Mastrogiovanni, G. Granozzi, E. Garfunkel, M. Chhowalla, *Adv. Funct. Mater.* **2009**, *19*, 2577.
[4] R. S. Sundaram, C. Gómez-Navarro, K. Balasubramanian, M. Burghard, K. Kern, *Adv. Mater.* **2008**, *20*, 3050.
[5] D. Voiry, J. Yang, J. Kupferberg, R. Fullon, C. Lee, H. Y. Jeong, H. S. Shin, M. J. S. Chhowalla, *Science* **2016**, *353*, 1413.
[6] S. Gilje, S. Dubin, A. Badakhshan, J. Farrar, S. A. Danczyk, R. B. Kaner, *Adv. Mater.* **2010**, *22*, 419.
[7] R. Larciprete, S. Fabris, T. Sun, P. Lacovig, A. Baraldi, S. Lizzit, *J. Am. Chem. Soc.* **2011**, *133*, 17315.
[8] N. Liu, F. Luo, H. Wu, Y. Liu, C. Zhang, J. Chen, *Adv. Funct. Mater.* **2008**, *18*, 1518.
[9] C. Liu, K. Wang, S. Luo, Y. Tang, L. Chen, *Small* **2011**, *7*, 1203.
[10] W. Chen, L. Yan, P. R. Bangal, *Carbon* **2010**, *48*, 1146.
[11] H. Hu, Z. Zhao, Q. Zhou, Y. Gogotsi, J. Qiu, *Carbon* **2012**, *50*, 3267.
[12] Z. Fan, K. Wang, T. Wei, J. Yan, L. Song, B. Shao, *Carbon* **2010**, *48*, 1686.
[13] Z.-J. Fan, W. Kai, J. Yan, T. Wei, L.-J. Zhi, J. Feng, Y.-M. Ren, L.-P. Song, F. Wei, *ACS Nano* **2011**, *5*, 191.
[14] X. Mei, J. Ouyang, *Carbon* **2011**, *49*, 5389.
[15] C. K. Chua, M. Pumera, *Chem. Soc. Rev.* **2014**, *43*, 291.
[16] D. Lin, Y. Liu, Z. Liang, H. W. Lee, J. Sun, H. Wang, K. Yan, J. Xie, Y. Cui, *Nat. Nanotechnol.* **2016**, *11*, 626.
[17] W. S. Hummers, R. E. Offeman, *J. Am. Chem. Soc.* **1958**, *80*, 1339.
[18] J. Liu, Z. Li, B. Jia, J. Zhu, W. Zhu, J. Li, H. Pan, B. Zheng, L. Chen, G. Pezzotti, J. Zhu, *J. Mater. Chem.* **2020**, *8*, 6303.
[19] M. Mahmudzadeh, H. Yari, B. Ramezanzadeh, M. Mahdavian, *J. Hazard. Mater.* **2019**, *371*, 609.
[20] N. A. Kumar, S. Gambarelli, F. Duclairoir, G. Bidan, L. Dubois, *J. Mater. Chem.* **2013**, *1*, 2789.
[21] A. Das, B. Chakraborty, A. K. Sood, *Bull. Mater. Sci.* **2008**, *31*, 579.
[22] C.-Y. Su, Y. Xu, W. Zhang, J. Zhao, X. Tang, C.-H. Tsai, L.-J. Li, *Chem. Mater.* **2009**, *21*, 5674.
[23] S. Stankovich, D. A. Dikin, R. D. Piner, K. A. Kohlhaas, A. Kleinhammes, Y. Jia, Y. Wu, S. T. Nguyen, R. S. Ruoff, *Carbon* **2007**, *45*, 1558.
[24] R. Liu, Y. Zhang, Z. Ning, Y. Xu, *Angew. Chem., Int. Ed.* **2017**, *56*, 15677.
[25] D. Akyüz, B. R. Keskin, U. Şahintürk, A. Koca, *Appl. Catal. B* **2016**, *188*, 217.
[26] P. Kumar, F. Shahzad, S. Yu, S. M. Hong, Y.-H. Kim, C. M. Koo, *Carbon* **2015**, *94*, 494.
[27] Q. Zhang, R. Tan, Y. Huang, H. Liang, *J. Loss Prev. Process. Ind.* **2012**, *25*, 982.
[28] V. K. Rao, M. F. Bardon, *Combust Flame* **1984**, *55*, 73.
[29] S. Zhang, N. Pan, *J. Mater. Chem.* **2013**, *1*, 7957.
[30] H. Feng, R. Cheng, X. Zhao, X. Duan, J. Li, *Nat. Commun.* **2013**, *4*, 1539.
[31] W. Gao, L. B. Alemany, L. Ci, P. M. Ajayan, *Nat. Chem.* **2009**, *1*, 403.
[32] Z. W. Seh, Y. Sun, Q. Zhang, Y. Cui, *Chem. Soc. Rev.* **2016**, *45*, 5605.
[33] Y. Li, S. Lin, D. Wang, T. Gao, J. Song, P. Zhou, Z. Xu, Z. Yang, N. Xiao, S. Guo, *Adv. Mater.* **2020**, *32*, 1906722.
[34] Z. Du, X. Chen, W. Hu, C. Chuang, S. Xie, A. Hu, W. Yan, X. Kong, X. Wu, H. Ji, L. J. Wan, *J. Am. Chem. Soc.* **2019**, *141*, 3977.
[35] H. Xu, Q. Jiang, B. Zhang, C. Chen, Z. Lin, *Adv. Mater.* **2020**, *32*, 1906357.
[36] F. Fabregat-Santiago, J. Bisquert, E. Palomares, L. Otero, D. Kuang, S. M. Zakeeruddin, M. Gratzel, *J. Phys. Chem.* **2007**, *111*, 6550.
[37] S. Evers, L. Nazar, *Chem. Commun.* **2012**, *48*, 1233.
[38] C. Wang, X. Wang, Y. Wang, J. Chen, H. Zhou, Y. Huang, *Nano Energy* **2015**, *11*, 678.
[39] C. Wang, X. Wang, Y. Yang, A. Kushima, J. Chen, Y. Huang, J. Li, *Nano Lett.* **2015**, *15*, 1796.